# Influence of sintering temperature, pressing, and conformal coatings on electron diffusion in electrophoretically deposited porous $TiO_2$

A. Ofir
*Bar-Ilan University, 52900 Ramat Gan, Israel*

Th. Dittrich
*Hahn-Meitner-Institute, Glienicker Strasse 100, 14109 Berlin, Germany*

S. Tirosh, L. Grinis, and A. Zaban[a)]
*Bar-Ilan University, 52900 Ramat Gan, Israel*

(Received 19 March 2006; accepted 20 July 2006; published online 11 October 2006)

The electrophoretic deposition of nanoporous $TiO_2$ layers allows us to investigate separately the influence of sintering temperature, porosity, and conformal surface coatings on the effective diffusion coefficient ($D_{\text{eff}}$) of excess electrons in porous layers. Photocurrent transients were measured to obtain $D_{\text{eff}}$ in nanoporous $TiO_2$ layers immersed in aqueous electrolyte. The applied treatments control parameters such as the contact between interconnected nanoparticles, the coordination of nanoparticles in the porous network, and the surface passivation of $TiO_2$ nanoparticles. The hierarchy of the different factors for transport optimization in porous $TiO_2$ is discussed. Under fixed geometry of the nanoporous network, trapping on surface states can strongly limit electron diffusion in porous $TiO_2$. © *2006 American Institute of Physics*.
[DOI: 10.1063/1.2356100]

## I. INTRODUCTION

Highly porous layers of metal oxide nanoparticles have become the focus of many recent investigations due to their large potential in various fields of applications such as batteries,[1] displays,[2] photocatalysis,[3] and solar energy conversion.[4] In most of these applications, electron transport plays an important role. The optimization of the transport in nanoporous metal oxide layers is a challenge due to the complexity of influencing factors which are related to the individual properties of nanoparticles and their electrical interconnects, to the local geometry, and to the huge internal surface area of a highly porous layer.

Porous metal oxide layers consist of a network of interconnected nanometer sized particles such as ZnO, $SnO_2$, $Nb_2O_5$, and $TiO_2$. The electrical interconnect between the metal oxide nanoparticles is usually realized by sintering at temperatures about 500 °C.[5] For specific applications, sintering at relatively high temperatures has to be avoided, for example, when polymers are used as substrates. An alternative to sintering at various temperatures, interconnects between metal oxide nanoparticles may be realized by applying high pressures which may induce locally a sintering process.[6] Another possibility to improve interconnects between metal oxide nanoparticles is the implementation of additional oxide material in the regions of necks between nanoparticles by wet chemical deposition techniques.[5]

The local geometry of porous metal oxide layers determines the percolation path of charge carriers. The mean coordination number between nanoparticles ($K$) is given by the porosity with respect to a random packing model.[7] The higher the value of $K$, the shorter the percolation path for electrons traveling in the porous network. For example, for film porosities of 50% and 75%, $K$ amounts to 4.5 and 2.5, while the fractions of terminating particles are 1% and 31%, respectively.[7] The critical porosity ($P_C$) is defined as the porosity above which closed percolation paths from one to the other contact become impossible. The value of $P_C$ has been analyzed, for example, for porous $TiO_2$ layers and amounts to $P_C=0.76$.[8] This is a very typical value for percolation in porous materials.[8]

The internal surface area of nanoporous metal oxides is of the order of 100 $m^2/cm^3$.[9] Therefore, even relatively low concentrations of surface states may strongly influence the charge transport due to trapping. Further, surface states may induce recombination of excess electrons with species in the electrolyte. In semiconductor physics, surface layers are used for electronic passivation. The most prominent one is the $Si/SiO_2$ system.[10] The surface passivation of metal oxide nanoparticles can be improved by coating the nanoparticle with an ultrathin layer of a metal oxide which has a larger bandgap than the nanoparticle, for example, by $Nb_2O_5$ (Ref. 11) or $Al_2O_3$ (Ref. 12) coatings on $TiO_2$ nanoparticles.

Usually, nanoporous metal oxide layers are prepared by screen printing of pastes containing organic binders and metal oxide nanoparticles followed by firing at high temperature in air to burn out the organic molecules.[13] During the firing, sintering of metal oxide nanoparticles fixes interconnects between nanoparticles and therefore the local geometry. For this reason, it is practically impossible to investigate separately the influence of factors such as interconnects and coordination and passivation of nanoparticles on transport phenomena such as electron diffusion.

Recently, we developed the electrophoretic deposition (EPD) technique for the preparation of nanoporous metal oxide layers.[14] The advantage of EPD is that the local geom-

[a)]Electronic mail: zabana@mail.biu.ac.il

 

TABLE I. Experimental conditions and overview of the investigated samples.

| Series | Variation and treatment | Laser | Sample | Layer thickness ($\mu$m) |
|---|---|---|---|---|
| A | Thickness by deposition time of EPD (after sintering at 500 °C | Nd:YAG (355 nm) 10 Hz 1.6 mJ/cm$^2$ | A1 | 1.2 (15 s) |
| | | | A2 | 2.9 (30 s) |
| | | | A3 | 4.6 (45 s) |
| | | | A4 | 9.5 (60 s) |
| | | | A5 | 10.5 (70 s) |
| | | | A6 | 12.5 (80 s) |
| | | | A7 | 15.3 (100 s) |
| B | Sintering temperature | $N_2$ (337 nm) 2 Hz 40 $\mu$J/cm$^2$ | B1 | 7.2 (300 °C) |
| | | | B2 | 7.2 (400 °C) |
| | | | B3 | 7.2 (500 °C) |
| | | | B4 | 7.2 (550 °C) |
| C | Pressure (after sintering at 500 °C) | $N_2$ (337 nm) 1 Hz 40 $\mu$J/cm$^2$ | C1 | 2.7 (unpressed) |
| | | | C2 | 2.2 (0.2 T/cm$^2$) |
| | | | C3 | 2.1 (0.4 T/cm$^2$) |
| | | | C4 | 1.95 (0.6 T/cm$^2$) |
| | | | C5 | 1.85 (0.8 T/cm$^2$) |
| D | $TiO_2$ coating time (before pressing at 0.8 T/cm$^2$ and unsintered) | Nd:YAG (355 nm) 10 Hz 1.6 mJ/cm$^2$ | D1 | 7.5 (uncoated) |
| | | | D2 | 7.5 (30 s) |
| | | | D3 | 7.5 (2 min) |
| E | MgO coating time (before pressing at 0.8 T/cm$^2$ and sintering at 500 °C) | Nd:YAG (355 nm) 10 Hz 1.6 mJ/cm$^2$ | E1 | 7.5 (uncoated) |
| | | | E2 | 7.5 (30 s) |
| | | | E3 | 7.5 (1 min) |
| | | | E4 | 7.5 (3 min) |

etry is not yet fixed after the formation of the porous layer. Therefore, interconnects between nanoparticles, local geometry, and surface passivation can be varied separately on porous metal oxide layers deposited by EPD.

Electron transport is determined by diffusion in porous metal oxides permeated with electrolyte since electrical fields are screened.[15] In transient photocurrent (PC) experiments, a porous metal oxide film is illuminated from the electrolyte side with light pulses which are strongly absorbed. Light-induced electrons diffuse through the porous metal oxide film towards the back contact were they are extracted at the interface and registered with a load resistance.[16] An effective diffusion coefficient ($D_{\text{eff}}$) can be obtained from the characteristic peak position ($t_{\text{peak}}$) of photocurrent transients and the film thickness ($L$):[16]

$$D_{\text{eff}} = \frac{L^2}{6t_{\text{peak}}}. \tag{1}$$

In this work, we apply the EPD technique for the deposition of nanoporous $TiO_2$ layers. Interconnects between $TiO_2$ nanoparticles are changed by variation of the sintering temperature. The local geometry of the nanoporous $TiO_2$ layers is modified by decreasing the porosity due to pressing. Conformal coating of $TiO_2$ nanoparticles by ultrathin $TiO_2$ and MgO layers is applied to vary necking and surface passivation. The effective diffusion coefficient and the integrated charge ($Q$) were measured by transient photoconductivity as a function of the various factors.

## II. EXPERIMENT

### A. Preparation of porous $TiO_2$ layers

Porous $TiO_2$ films were fabricated by cathodic EPD method developed in our laboratory and described elsewhere by Grinis *et al.*[14] EPD enables simple preparation of uniform, binder-free films with controlled thickness and with high reproducibility. The $TiO_2$ particles (P25, Degussa) were deposited on a conducting glass [$SnO_2$:F, 8 $\Omega/\square$, Libby Owens Ford (LOF)]. The thicknesses of the porous $TiO_2$ films were measured with a surftest SV 500 profilometer of Mitutoyo Co. Five series of electrodes were prepared (summarized in Table I).

Series A (thickness variation) contained seven porous $TiO_2$ layers with thicknesses between 1.2 and 15 $\mu$m. One can see from the comparison of the layer thicknesses with the deposition time that the thickness of the porous $TiO_2$ layers is well controlled by the deposition time. The porous $TiO_2$ films were sintered at 500 °C in air for 30 min.

Series B (variation of the annealing temperature) contained four porous $TiO_2$ layers with identical thickness. The porous $TiO_2$ layers were sintered at 300, 400, 500, and 550 °C in air for 30 min.

Series C (pressure treatment) contained one unpressed porous $TiO_2$ layer and four porous $TiO_2$ layers pressed at 0.2, 0.4, 0.6, and 0.8 $T/cm^2$ before sintering at 500 °C in air for 30 min. A hydraulic programmable press (Bivas Hydraulic Industries Ltd.) was used for pressing at room temperature. Pressing leads to a reduction of the layer thickness and therefore to a decrease of the porosity. The porosities of the pressed layers were obtained from $P_p=(L_p-0.4L_{np})/L_p$, where $L_p$ and $L_{np}$ are the thicknesses of the pressed and unpressed layers, respectively, and amounted to 0.6, 0.51, 0.49, 0.45, and 0.42 $T/cm^2$ for the unpressed and 0.2, 0.4, 0.6, and 0.8 $T/cm^2$ for the pressed nanoporous $TiO_2$ layers, respectively.

Series D (conformal $TiO_2$ coating) contained three porous $TiO_2$ layers; one uncoated and two coated at different times. The porous $TiO_2$ layers were pretreated by pressing at 0.8 $T/cm^2$ before coating in tetraisopropyl ortotitanate based alcoholic solution was performed. The coating time is directly related to the thickness of the ultrathin $TiO_2$ layer and can be changed from few angstroms to a few nanometers. All three porous $TiO_2$ layers were only dried (not sintered) at 150 °C in air for 1 h after coating.

Series E (conformal MgO coating) contained four porous $TiO_2$ layers; one uncoated and three coated at different times. The porous $TiO_2$ layers were pretreated by pressing at 0.8 $T/cm^2$ before coating in magnesium ethoxide alcoholic solution was performed. All four porous $TiO_2$ films were sintered in air at 500 °C for 30 min after coating.

### B. Measurement of photocurrent transients

The measurements were performed in a homemade electrochemical cell made of Teflon which was electrostatically screened by a Faraday cage.[15] The samples were sealed with an O-ring (diameter of 7 mm) and illuminated from the electrolyte side. The electrolyte was aqueous 0.5*M* NaCl with *p*H=2 (HCl). Two different lasers were used for the experiments. The excess charge carriers for series A, D, and E were generated by pulses of the third harmonic of a Nd:YAG (yttrium aluminum garnet) laser (wavelength of 355 nm, duration of the laser pulse of 150 ps, intensity of 1.66 $mJ/cm^2$, and repetition rate of 10 Hz). Series B and C were measured with a $N_2$ laser (wavelength of 337 nm, duration of the laser pulse of 5 ns, intensity of 40 $\mu J/cm^2$, and repetition rate of 2 or 1 Hz). The measurement resistance was 50 Ω. The measurements were performed in a quasistationary regime. The photocurrent transients were measured at only one fixed excitation light intensity despite the fact that the effective diffusion coefficient depends usually on the light intensity. Nevertheless, our measurement regime was sufficient for comparing the general trends of $D_{eff}$ and $Q$ between samples within one series or between series D and E.

## III. RESULTS AND DISCUSSION

### A. Thickness dependence

Figure 1 shows some PC transients for nanoporous $TiO_2$ layers of series A on a logarithmic time scale. The onset of the laser pulse is shifted to 70 ns. The peak of the photocurrent transients shifts to shorter times with decreasing film thickness, as expected. The correlation between the square of the thickness and the peak time ($t_{peak}$) is plotted in the insert of Fig. 1. The linear dependence with the slope shows that $t_{peak}$ is dominated by one effective diffusion coefficient ($D_{eff}=10^{-5}$ $cm^2/s$ under the given measurement conditions) over the whole range of thicknesses. Therefore, it can be concluded that the nanoporous $TiO_2$ layers are homogeneous over the whole thickness and that anomalous diffusion does not control the peak position of the photocurrent transients under the given conditions. This conclusion is used in the analysis of the following experiments when $D_{eff}$ is determined from $t_{peak}$ of one photocurrent transient obtained on a nanoporous $TiO_2$ layer with a known thickness.

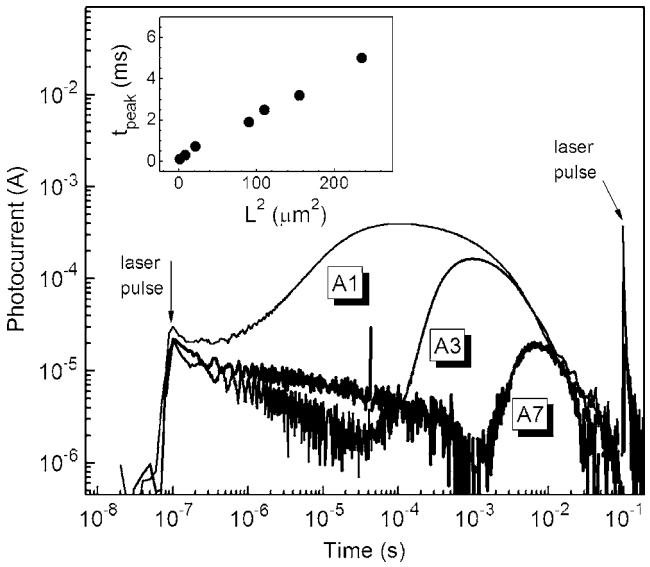


FIG. 1. Characteristic photocurrent transients for samples with three thicknesses. The insert shows the correlation between the peak time of the transients and the squared thickness.

With increasing film thickness, the charge integrated over the photocurrent transients decreases by up to a factor of 2. The repetition rate cuts the decays of the photocurrent transients and leads to a steady state population of the deepest traps. The relative influence of the cutting of the transients increases with increasing layer thickness, resulting in the decrease of $Q$. Therefore, nanoporous $TiO_2$ layers with thicknesses in the same range were used for the following experiments in order to compare changes of recombination and trapping after different treatments. We note that $t_{peak}$ is practically not influenced by recombination as long as the electron life time is of the same order as $t_{peak}$. Under these conditions $Q$ is much more sensitive to recombination. In contrast, trapping influences $t_{peak}$ much stronger than it affects $Q$.[17]

### B. Influence of the sintering temperature

Figure 2 summarizes the measurements on the nanoporous $TiO_2$ layers of series B as the dependence of $t_{peak}$ and $Q$ on the sintering temperature. The value of $D_{eff}$ is inverse proportional to $t_{peak}$ since the thicknesses of the films are identical. The results demonstrate the increase of $D_{eff}$ with increasing sintering temperatures. The value of $Q$ remains

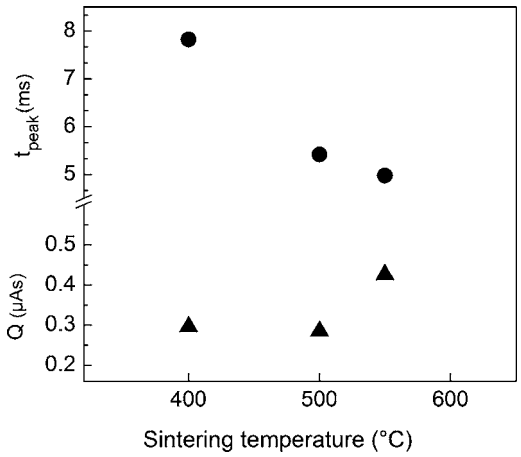


FIG. 2. Dependence of the peak time and of the integrated charge on the sintering temperature.

constant within the experimental error for lower sintering temperatures and increases by about 30% after sintering at 550 °C. The decrease of $t_{peak}$ concomitant with the increase of $Q$ demonstrates also that $t_{peak}$ is dominated by $D_{eff}$. It is important to note that no signal was observed for the nanoporous $TiO_2$ layer sintered at 300 °C. This indicates the necessity of a heat treatment at temperatures significantly higher than 300 °C for getting a reasonable interconnect between $TiO_2$ nanoparticles deposited by the EPD technique.

As already shown by Kambe *et al.*,[5] the film morphology of nanoporous $TiO_2$ layers does not change significantly with the annealing temperature (between 400 and 550 °C). Therefore, the sintering affects mostly interconnects between particles. Increasing particle necking without changing the pores size and film morphology enables the raising of $D_{eff}$ without damaging the collection properties of the films. The significance of increasing the annealing temperature up to 550 °C for improving the necking between particles underlines the problems which one has to overcome in order to design and manufacture films on plastic substrates.

### C. Role of the pressure treatment

Figure 3 shows secondary electron microscopy (SEM) micrographs of the unpressed and pressed with 0.8 T/cm$^2$ nanoporous $TiO_2$ layers. After pressing, larger pores and pronounced agglomerates disappear as the film becomes denser and more homogeneous. This clearly demonstrates that the local geometry of nanoporous metal oxide layers can be changed systematically by pressing.

With increasing pressure, the porosity decreases, which leads also to a decrease of the penetration depth of the excitation light in the nanoporous $TiO_2$ layer. Further, light scattering experiments showed that the medium roughness of nanoporous $TiO_2$ layers deposited by EPD decreased after pressing.[18] This gives an additional decrease of the penetration depth of the excitation light in the nanoporous $TiO_2$ layer. With respect to the penetration depth of the excitation light and its change due to changed porosity and roughness after pressing, one has to consider a reduced effective thickness of the nanoporous $TiO_2$ layer when calculating $D_{eff}$. For the calculation of $D_{eff}$, $L$ has been reduced by $\alpha^{-1}/(1\text{-}P)$, where $\alpha^{-1}$ is the penetration depth of the light (about 0.4 $\mu$m in $TiO_2$ for the given wavelength) and $P$ is the porosity.

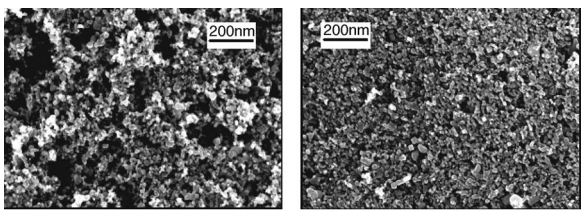


FIG. 3. Micrographs of the top views of unpressed porous $TiO_2$ layer deposited by EPD (a) and of a nanoporous $TiO_2$ layer after pressing (b).

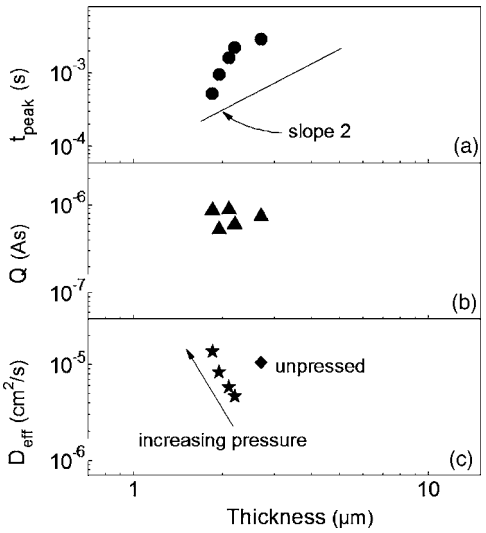


FIG. 4. Thickness dependence of the peak time (a), the integrated charge (b), and the effective diffusion coefficient (c) for the unpressed and pressed with different pressures nanoporous $TiO_2$ layers. The line in (a) represents a slope of 2. Note the increase of the effective diffusion coefficient with increasing pressure of the pressed nanoporous $TO_2$ layers (c).

Figure 4 shows the dependences of $t_{peak}$, $Q$, and $D_{eff}$ on the thickness of the nanoporous $TiO_2$ layers of series C. For the pressed nanoporous $TiO_2$ layer, the most striking feature is that $t_{peak}$ decreases much stronger with decreasing $L$ than one would expect for diffusion with a diffusion constant that is independent of $L$. Therefore, $D_{eff}$ increases with decreasing $L$ for the pressed nanoporous $TiO_2$ layers as shown in Fig. 4(c). Such behavior can be understood in terms of percolation in a porous network with increasing coordination number between interconnected nanoparticles.[19] As remark, an influence of recombination or modified trapping on $t_{peak}$ can be ruled out since the integrated charge is independent of $L$ [Fig. 4(b)] for the given set of samples.

It is important to notice that $D_{eff}$ of the unpressed nanoporous $TiO_2$ layer is significantly larger than $D_{eff}$ of the nanoporous $TiO_2$ layers pressed at low pressures. This is not an artifact and points to the effect of partial ordering in nanoporous $TiO_2$ layers deposited by EPD.[20] The partial ordering induced by EPD is lost during pressing.

### D. Conformal $TiO_2$ coating of pressed but unsintered nanoporous $TiO_2$ layers

One question is whether sintering at relatively high temperatures can be avoided, for example, by necking of nano-

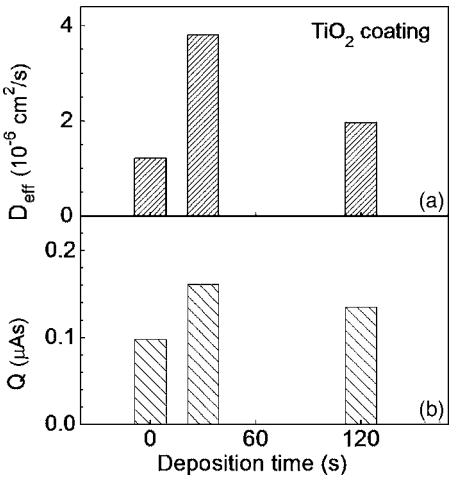


FIG. 5. Dependence of the effective diffusion coefficient (a) and the integrated charge (b) on the deposition time of the $TiO_2$ coating layer, i.e., its thickness.

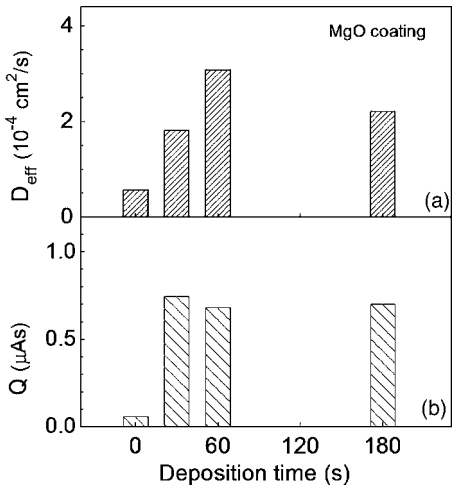


FIG. 6. Dependence of the effective diffusion coefficient (a) and the integrated charge (b) on the deposition time of the MgO coating layer, i.e., its thickness.

particles in chemical solutions in which ultrathin $TiO_2$ layers can be deposited at $TiO_2$ surfaces. The ultrathin $TiO_2$ coating was expected to form good necking between $TiO_2$ particles and thus enable electron transport through the porous layers in cases when the layers were neither pressed nor sintered. However, unpressed nanoporous $TiO_2$ layers did not give any photocurrent response irrespective to $TiO_2$ coating. We believe that electronic states are different in $TiO_2$ nanoparticles and in ultrathin $TiO_2$ layers, which causes the formation of additional barriers for electron transport at interconnects between $TiO_2$ nanoparticles.

Electron diffusion in unsintered nanoporous $TiO_2$ layers could be observed only on layers which were pressed at the highest pressure, i.e., 0.8 $T/cm^2$. These PC transients had to be measured at an intensity of the laser pulses as large as 1.6 $mJ/cm^2$. Figure 5 shows the values of $D_{eff}$ and $Q$ obtained on the unsintered and uncoated and coated with ultrathin $TiO_2$ nanoporous $TiO_2$ layers pressed at 0.8 $T/cm^2$. The values of $D_{eff}$ and $Q$ of the uncoated layer amount to about $1\times10^{-6}$ $cm^2/s$ and 0.1 $\mu$As, respectively, under the given conditions.

Coating for 30 s leads to an increase of $Q$ by about 50% while $D_{eff}$ increased by more than three times. Since the ultrathin $TiO_2$ coating is unimportant for better interparticle transport between $TiO_2$ nanoparticles, it can be concluded that $TiO_2$ coating for 30 s improved the surface passivation of $TiO_2$ nanoparticles from the point of view of reduced trapping. This seems surprising since one would expect even increased trapping at $TiO_2$ surfaces which are not treated at high temperatures. One has to consider that the ultrathin $TiO_2$ layer and the pressed $TiO_2$ nanocrystallites have different electronic structures, resulting, for example, in an offset of the conduction bands. However, other experiments are needed to get a deeper understanding of this point. For longer times of coating, however, the values of $D_{eff}$ and $Q$ decrease significantly. We assume that the passivating properties of the ultrathin $TiO_2$ coating diminish with increasing thickness due to the development of stress in the layer, leading to the development of surface defects. Therefore, the thickness of passivation layers is a very critical issue and has to be investigated more detailed in future.

### E. Conformal MgO coating of pressed and sintered nanoporous $TiO_2$ layers

The value of $D_{eff}$ of the pressed at 0.8 $T/cm^2$ and sintered at 500 °C nanoporous $TiO_2$ layer increased by about 50 times in comparison to the unsintered one, whereas $Q$ remained practically unchanged (compare the values at 0 s in Figs. 5 and 6). This allows us to draw two conclusions: first, the formation of *well sintered* intimate interconnects between $TiO_2$ nanoparticles is the most important factor for electron diffusion, and second, surface states being responsible for electron recombination are not directly related to trap states which only limit the electron diffusion.

An important question is whether both kinds of surface states, recombination centers and electron traps, can be effectively passivated by ultrathin MgO coatings. This question is addressed in Fig. 6. In this experiment, the thermal load was the same for all samples. The value of $Q$ increased by seven to eight times after MgO coating independent on the coating time. Therefore, the thickness of the MgO passivation layer is not important for the passivation of recombination centers at the $TiO_2$ surface. The dependence of $D_{eff}$ on the MgO coating time is more complicated. The value of $D_{eff}$ increased to about $2\times10^{-4}$ $cm^2/s$ after MgO coating for 30 s. With increasing MgO coating time to 60 s, $D_{eff}$ increased even further to about $3\times10^{-4}$ $cm^2/s$. Therefore, MgO passivates $TiO_2$ surfaces very efficiently. However, longer MgO coating times cause a significant decrease of $D_{eff}$ towards $2\times10^{-4}$ $cm^2/s$. The reason for this behavior is not well understood yet. We believe that the influence of ionic charge incorporated in the MgO coating has to be considered.

## IV. SUMMARY

Our results on nanoporous $TiO_2$ layers prepared by EPD show that a hierarchy of four processes has to be considered

for the optimization of electron diffusion. The first process is the deposition of the nanoporous $TiO_2$ layers by EPD, which opens general opportunities for optimization of electron diffusion in such layers. The second process aims to the geometrical factor in interconnected porous networks. By pressing, the porosity of nanoporous $TiO_2$ layers deposited by EPD can be decreased and thus the coordination number between $TiO_2$ nanoparticles can be increased, which improves percolation. The third process, the sintering at relatively high temperatures, is the most important one since it is responsible for creating intimate interconnects between $TiO_2$ nanoparticles. Pressing alone is not sufficient for getting good electron diffusion in nanoporous $TiO_2$ layers. This gives a principal limitation for the application of nanoporous $TiO_2$ layers on plastics which cannot be treated at high temperatures. The fourth process contains a coating procedure (with MgO) in order to passivate recombination centers and trap states at the surfaces of interconnected $TiO_2$ nanoparticles. Our experiments showed that trapping of electrons at surface states can strongly limit the electron diffusion in nanoporous $TiO_2$ and that the trap density is much higher at the $TiO_2$/electrolyte interface than at the $TiO_2$/MgO interface. The coating procedure has to be optimized very carefully since it determines also the injection properties of electrons from adsorbed dye molecules for dye sensitized solar cells.

## ACKNOWLEDGMENTS

The authors are grateful to Professor J. Bisquert for discussions and A. Belaidi for making the SEM micrographs.

[1] S. Huang, L. Kavan, I. Exnar, and M. Grätzel, J. Electrochem. Soc. **142**, L142 (1995).
[2] M. O. M. Edwards, G. Boschloo, T. Gruszecki, H. Pettersson, R. Sohlberg, and A. Hagfeldt, Electrochim. Acta **46**, 2187 (2001).
[3] In *Sol-Gel Processed* $TiO_2$*-Based Materials for Solar Cells, Photocatalysts and Other Applications*, special issue of J. Sol-Gel Sci. Technol. **22**, 5 (2001).
[4] B. O'Regan and M. Grätzel, Nature (London) **353**, 737 (1991).
[5] S. Kambe, S. Nakade, Y. Wada, T. Kitamura, and S. Yanagida, J. Mater. Chem. **12**, 723 (2002).
[6] H. Lindstrom, A. Holmberg, E. Magnusson, S. E. Lindquist, L. Malmqvist, and A. Hagfeldt, Nano Lett. **1**, 97 (2001).
[7] J. van de Lagemaat, K. D. Benkstein, and A. J. Frank, J. Phys. Chem. B **105**, 12433 (2001).
[8] K. D. Benkstein, J. Kopidakis, J. van de Lagemaat, and A. J. Frank, J. Phys. Chem. B **107**, 7759 (2003).
[9] L. Kavan, M. Grätzel, J. Rathousky, and A. Zukal, J. Electrochem. Soc. **143**, 394 (1996).
[10] C. Robert Helms and B. E. Deal, *Physics and Chemistry of* $SiO_2$ *and the* $Si/SiO_2$ (Plenum, New York, 1989).
[11] A. Zaban, S. G. Chen, S. Chappel, and B. A. Gregg, Chem. Commun. (Cambridge) **2000**, 2231.
[12] Th. Dittrich *et al.*, Appl. Surf. Sci. **240**, 236 (2005).
[13] P. V. Kamat, in *Molecular Level Artificial Photosynthetic Materials*, edited by K. D. Karlin (Wiley, New York, 1997), pp. 273–343.
[14] L. Grinis, A. Ofir, and A. Zaban (unpublished).
[15] A. Zaban, A. Meier, and B. A. Gregg, J. Phys. Chem. B **101**, 7985 (1997); S. Rühle and Th. Dittrich, *ibid.* **109**, 9522 (2005).
[16] A. Solbrand, H. Lindström, H. Rensmo, A. Hagfeldt, and S.-E. Lindquist, J. Phys. Chem. B **101**, 2514 (1997).
[17] For more details see also S. Rühle and Th. Dittrich, J. Phys. Chem. B **110**, 3883 (2006).
[18] A. Ofir, T. Dittrich, S. Dor, and A. Zaban (unpublished).
[19] T. Dittrich, A. Ofir, S. Tirosh, L. Grinis, and A. Zaban, Appl. Phys. Lett. **88**, 182110 (2006).
[20] S. Tirosh, T. Dittrich, A. Ofir, L. Grinis, and A. Zaban, J. Phys. Chem. B **110**, 16165 (2006).